

Scientific paper

A 320 k-year record of microparticles in the Dome Fuji, Antarctica ice core measured by laser-light scattering

Yoshiyuki Fujii¹, Mika Kohno¹, Sumito Matoba², Hideaki Motoyama¹
and Okitsugu Watanabe¹

¹ National Institute of Polar Research, Kaga 1-chome, Itabashi-ku, Tokyo 173-8515

² National Institute for Environmental Studies, Onogawa, Tsukuba 305-8506

Abstract: A laser-light scattering method was evaluated from the viewpoint of the measurement ability of concentration and size distribution of microparticles in molten ice core samples. It was demonstrated that analysis can be performed with 10% accuracy by diluting the sample with ultrapure water by 50 times to eliminate coincidence loss. Using this method, the concentration and size distribution of microparticles were determined on 2829 samples from a 2503 m deep ice core drilled at Dome Fuji, Antarctica. The present paper shows the profiles of number and volume concentrations through the whole depth and the changes in the size distribution through three glacial cycles in the past 320 k-years.

key words: microparticle, core, laser, Dome-F, Antarctica

1. Introduction

Ice sheets in polar regions contain solid microparticles derived from land area in the past. These provide valuable information related to changes in land area environment and atmospheric circulation. Studies have been performed on solid microparticles in ice cores from various viewpoints such as long term variations including the last glacial (Thompson and Mosley-Thompson, 1981; Petit *et al.*, 1981, 1999; De Angelis *et al.*, 1984; Steffensen, 1997; Delmonte *et al.*, 2002), decadal to centennial time scale variations (Mosley-Thompson and Thompson, 1982; Maggi and Petit, 1998; Fujii *et al.*, 2001), seasonal changes (Thompson *et al.*, 1975; Fujii and Ohata, 1982; Steffensen, 1988; Ram and Koenig, 1997), dust source area (De Angelis *et al.*, 1992; Biscaye *et al.*, 1997; Basile *et al.*, 1997), optical depth of dust (Royer *et al.*, 1983), interaction between climatic variations and terrestrial environment changes (Grousset *et al.*, 1992; Zielinski and Mershon, 1997; Steffensen, 1997), and so on.

Detailed records of microparticles in ice cores in Antarctica have been obtained on decadal to millennial time scales (Gliozzi, 1966; Mosley-Thompson and Thompson, 1982; Mumford and Peer, 1982; Fujii and Watanabe, 1988; Maggi and Petit, 1998). However, few studies have been carried out on microparticle on the time scale of glacial cycles (Petit *et al.*, 1999). Detailed long-term changes of dust concentration in ice cores are essential to evaluate the roles of dust in terrestrial environment change and in climate change during glacial and interglacial cycles.

In the present study, we evaluated the details of concentration and size distribution of microparticles in the 2503 m deep ice core from Dome Fuji, Antarctica. Up to the present, a Coulter Counter has been widely used for the analysis of microparticles in ice cores (Thompson and Mosley-Thompson, 1981; Petit *et al.*, 1981; Fujii and Watanabe, 1988; Steffensen, 1997; Maggi and Petit, 1998; Delmonte *et al.*, 2002). However, when seen from such viewpoints as prevention of contamination in pre-treatment of the sample or influence of noise during measurement of analytical values, this is not the best method for the purpose. For decontamination purposes the inner section of the NGRIP Greenland ice core was used for high resolution particle analysis with a laser light scattering method on a flow-through basis (Ruth, 2002; Ruth *et al.*, 2002). In our present study, we use a light-scattering laser particle counter on a batch basis instead of a Coulter Counter to minimize contamination and miscounting. We here verify the useful features of analysis using of the laser particle counter.

2. Analysis

2.1. Pre-treatment

The ice core obtained at Dome Fuji was cut into three pieces: A, B and C, representing 60%, 25% and 15% of the horizontal cross-section, respectively. Core C was used for analyses of the microparticles, major chemical components, pH, and electrical conductivity. For the analysis, the core C sample was cut to 7 cm in length in a low temperature laboratory. A surface layer about 5 mm in thickness was removed in a clean bench using a ceramic knife, and a sample piece thus cut off was placed into a pre-cleaned polypropylene container.

Then, the surface several mm was washed off using ultrapure water in a clean room of class 10000 at room temperature, and the sample was placed into a polypropylene container rinsed in advance and was spontaneously thawed. For microparticle analysis, 1 ml of each sample was placed into a glass container after thawing using an auto-pipette, and was diluted with 50 ml of ultrapure water. The polypropylene container, the glass bottle, and the auto-pipette tip had been washed with ultrapure water for 20 min using ultrasonic waves. The procedure is summarized in Section 2.2.7.

2.2. Analysis using the laser particle counter

2.2.1. Principle of measurement

For the analysis, a laser particle counter (Met One Model-211 with high concentration sensor) installed in the clean room was used (Fig. 1). This counter is a scattering type counter using infrared laser light from a semiconductor laser diode. Light scattering sensors detect smaller particles than light-blocking sensors and are more effective at counting light-colored particles (Met One, 1991). The light scattered by the particles is focused on a photo diode through a lens, and the intensity of light is measured. The intensity of the scattered light is proportional to the size of the particles. Also, the number of pulses of scattered light indicates the number of particles. The photo diode converts the detected scattered light to electric pulses and sends the pulses to a pulse counter. Figure 2 is a schematic drawing to show the principle of detection. Table 1 gives the major specifications of the laser particle counter.



Fig. 1. A light scattering laser particle counter (Met One Model-211) located in a class 10000 clean room.

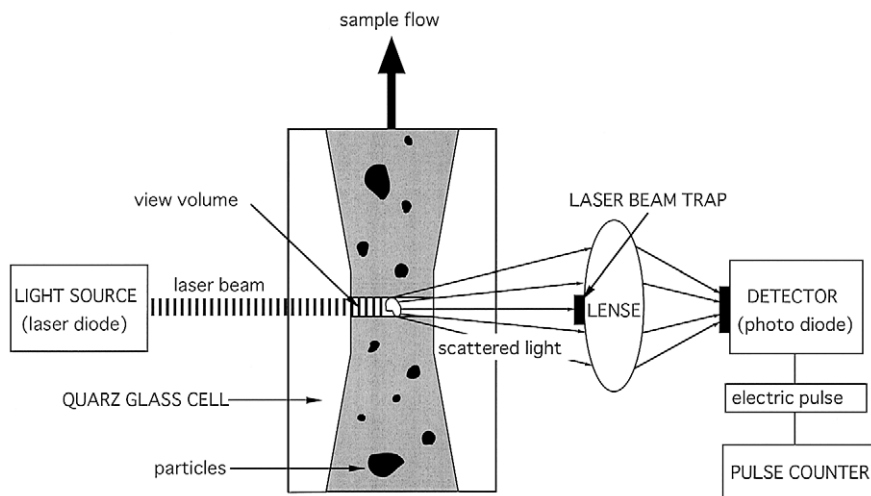


Fig. 2. A light scattering laser particle sensor.

Table 1. Specification of light-scattering laser particle counter (Met One Model-211 with high concentration sensor).

Item	Specification
Light source	Infrared laser diode
Laser life	Up to 300,000 hours
Dynamic range	0.5–25 μm
Flow rate	50 ml min^{-1}
Coincidence error	Less than 10% at 10500 particles ml^{-1}
Sensor supply voltage	+15 V, -15 V (DC)

2.2.2. Measurements of particle concentration by Coulter Counter and laser particle counter

For measurement of concentration of microparticles, the Coulter Counter has been used by many scientists. The present authors have also used the Coulter Counter (Model TA-II) for measurements of concentration and size distribution of microparticles in a 700 m Mizuho ice core from Antarctica (Fujii and Watanabe, 1988), a shallow ice core from Greenland (Fujii *et al.*, 2001) and Antarctic surface snow samples (Fujii and Ohata, 1982). Both types of counters have advantages and disadvantages. When a Coulter Counter is used, it is necessary to add salt solution such as NaCl to make the sample electrolyzed. The filtering and adding of this solution may cause contamination. Also, the sample and the electrolytic solution to be added must be accurately weighed in order to maintain the electrolyzed state of the sample at a constant level, this requires much time. Further, electric noise of background level hinders the measurement of smaller size particles even when the measuring apparatus is placed in a shield case and is electrically grounded.

Hammer (1977), Petit *et al.* (1981), and Ram and Koenig (1997) introduced a light scattering technique to measure relative dust concentration in polar ice meltwater. This is a rapid and effective technique but provides only relative particle concentration. In other words, this is generally not suitable for the measurement of number/volume concentration and size distribution for samples because coincidence loss is induced when a plurality of particles in a high particle concentration sample enters the view volume shown in Fig. 2. For this reason, the laser particle counter had not been used for the measurement of microparticle concentration and size distribution of ice core meltwater except in a few recent works (Ruth, 2002; Ruth *et al.*, 2002). In the present study, we show that the measurement of microparticles by using the light-scattering particle counter is possible within the accuracy of 10% by diluting the sample with ultrapure water since the measurable maximum concentration of the laser particle counter used, Met One Model-211, is 10500 particles per ml within the coincidence error of 10%.

2.2.3. Time for measurement

In the laser particle counter used in the present study, the measurement time can be set to one second or more in the unit of whole seconds. To increase the accuracy of measurement for the limited quantity of samples, it is necessary to increase the number of measurements. We changed the measurement time for the same sample to find out how far the measurement time can be shortened. As a result, it was found that sufficient measurement could be made even when the measurement time was set to 2 s (Fig. 3). The pause between measurements is fixed to 1 s.

2.2.4. Checking by standard particles

To check the particle size measurement by this laser particle counter, standard size of latex beads with number modal diameters of 0.492 μm , 1.089 μm and 1.868 μm were used. Because the concentration of the standard particle is not known, it was diluted with ultrapure water so that the concentration was within the maximum measurable concentration of this apparatus. The results are shown in Fig. 4. Figure 4a shows the size distribution of the three standard particle samples when measured separately. Figure 4b represents the results of the measurement on samples which were prepared by combining equal amounts of the three standard particle samples from Fig. 4a. Compared with Fig. 4a, particle size distribution is shifted toward larger particle size. This is caused by coincidence. The coincidence loss is

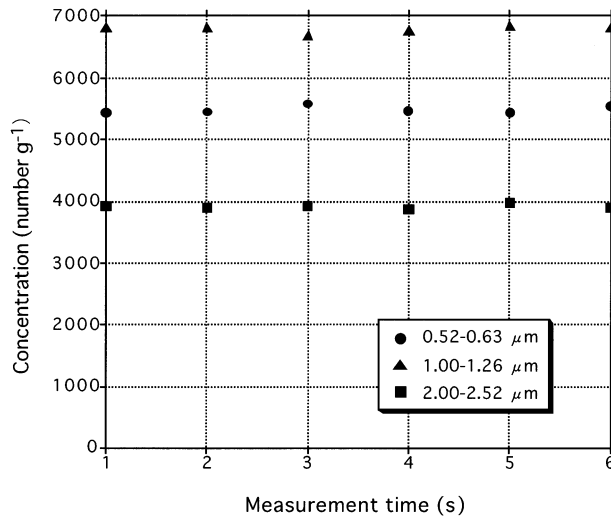


Fig. 3. Microparticle number concentration for particle sizes of 0.52–0.63, 1.00–1.26, and 2.00–2.52 μm when measurement time is changed.

caused by that the scattered light from particles is turned to a single scattering event when there are two or more particles in the sensor view volume. Figure 4c shows the background particle distribution of ultrapure water, which is used to dilute samples, obtained by 100 continuous measurements. Figure 4d shows the results of measurement when the mixed standard particle sample is diluted with ultrapure water by 50 times in order to prevent coincidence loss. This result is closer to the size distribution pattern shown in Fig. 4a and it means that there is no more coincidence loss. This indicates the importance of setting the particle concentration in the sample to be measured within the measurable concentration.

2.2.5. Dilution factor

Microarticle concentration in the core obtained in Antarctica exceeds the measurable concentration of this particle counter (10500 particles per m^3 when coincidence error is within 10%). For this reason, it is necessary to dilute the sample with ultrapure water to eliminate the influence of coincidence loss. When dilution is used, the microparticle concentration of the core sample must be obtained by subtracting the number of microparticles in ultrapure water used for dilution from the measured value obtained in the diluted sample. In this respect, the higher the dilution factor is, the more the analysis error increases due to the increase of measurement error in the particle concentration in the ultrapure water. Therefore, an optimal dilution factor must be determined from two viewpoints: influence of coincidence loss and measurement error.

1) Influence of coincidence loss

The influence of coincidence loss was evaluated by using a molten Dome Fuji ice core sample from 1127.97 m depth during a stadial of the last glacial. Figure 5 shows the total number concentration of particles larger than 0.52 μm in diameter when the dilution factor was varied to 0, 10, 20, 30, 50, 75, 100 and 200 times. As is clear from this figure, with the increase of the dilution factor, the measured number concentration increases. When the dilution factor exceeds 50 times or more, microparticle concentration reaches almost a constant

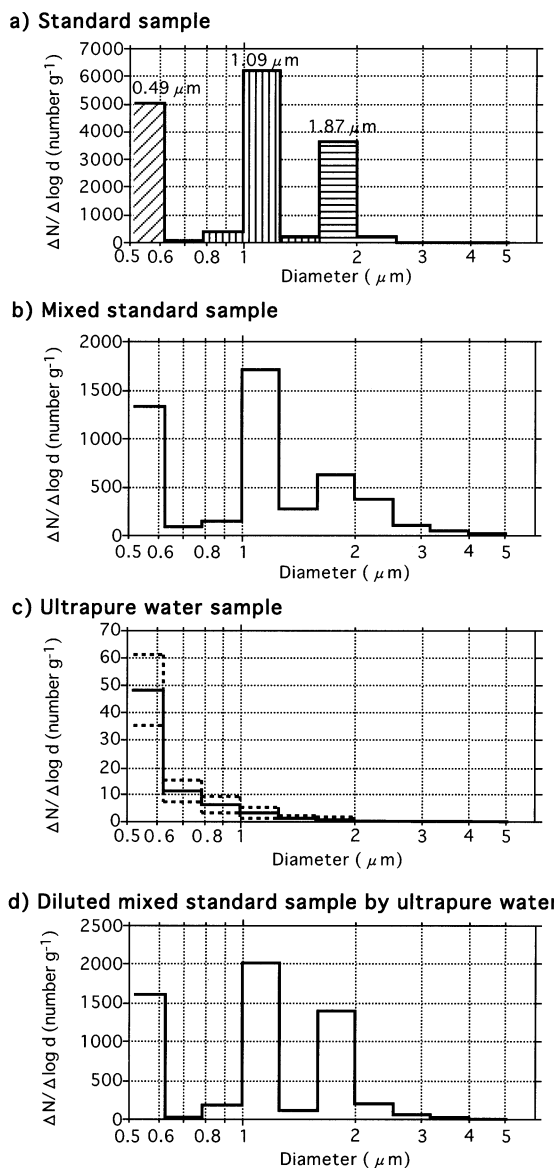


Fig. 4. a) Check on the ability of a laser particle counter with standard particles with number modal diameters of 0.492 μm , 1.089 μm and 1.868 μm . Measurements done separately for the standard particle samples show the proper size distribution. b) Coincidence loss appears when the same quantity of standard particle samples used for a) are mixed. c) The background particle distribution of ultrapure water, which is used to dilute mixed samples of b), obtained by 100 continuous measurements. Dashed lines show the probable error. d) Coincidence loss of the mixed sample used for b) disappears when it is diluted 50 times by ultrapure water.

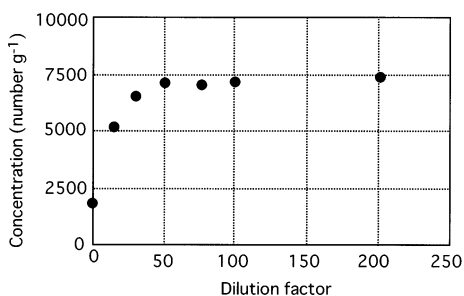


Fig. 5. Check on coincidence loss by changing the dilution factor for samples. Total number concentration of microparticles larger than 0.52 μm in diameter increases with dilution factor up to 50 times and then reaches almost a constant value suggesting that there is no influence of coincidence loss when the sample is diluted by 50 times or more.

value suggesting no influence of coincidence loss. Therefore, from the viewpoint of the influence of coincidence loss, this indicates that the dilution factor must be set to 50 times or more.

2) Measurement error

The microparticle concentration C of the molten core sample is expressed by the following equation:

$$C = \left\{ C_m - \left(1 - \frac{1}{x} \right) \cdot C_b \right\} \cdot x, \quad (1)$$

where x denotes the dilution factor, C_b is the concentration of the microparticles in ultrapure water, and C_m is the concentration of the microparticles in a mixed solution of ultrapure water and the molten sample.

The measurement accuracy of the particle concentration C of the molten sample calculated from eq. (1) is determined by uncertainties of x and C_b , and by the probable error of C_m . The probable measurement error r_c of the microparticle concentration in the molten core sample is given by the following equation according to the law of propagation of errors:

$$r_c = \sqrt{\left(\frac{\partial C}{\partial x} \right)^2 \cdot r_x^2 + \left(\frac{\partial C}{\partial C_m} \right)^2 \cdot r_{c_m}^2 + \left(\frac{\partial C}{\partial C_b} \right)^2 \cdot r_{c_b}^2}, \quad (2)$$

where r_x is the probable error of dilution factor, and r_{c_m} and r_{c_b} are the measurement probable errors of the microparticles in the mixed solution and in ultrapure water, respectively.

From 100 consecutive measurements of the same sample of ultrapure water and standard particles, the measurement probable errors (r_{c_m} and r_{c_b}) and the concentration of microparticles in ultrapure water (C_b) are obtained. Using these values, the relative probable error (r_c/C) of the molten sample is calculated by eq. (2).

Figure 6 shows the relation between the relative probable error (r_c/C) of the molten sample and the dilution factor (x) using the microparticle concentration C of the molten sample as a parameter. For the microparticle concentration C , we refer to the Vostok ice core data (De Angelis *et al.*, 1984). As is apparent from Fig. 6, the higher the dilution factor, the greater the relative probable error. When the dilution factor is 50, the relative probable error is 10% or lower.

Based on the above evaluation of the influence of coincidence loss and the relative probable error, the dilution factor of the sample was set to 50.

2.2.6. Check by SEM

For the purpose of checking the measurement coincidence loss of the sample diluted 50 times, the particle size distribution was measured for the samples of the last glacial at 521 m depth of the Dome Fuji ice core by using SEM imaging (Fig. 7) magnified 7000 times. The sample was filtered through a nuclepore filter with pore diameter of 0.22 μm . The measurement of particle size was carried out using 6 SEM images. Figure 8a shows the size-number and size-volume distributions of microparticles larger than 0.25 μm in diameter based on the SEM images. The number concentration has a modal diameter between 0.40 and 0.52 μm . This SEM result is a bit different from the size distribution peak of 0.50–1.0 μm in the Vostok ice core (De Angelis *et al.*, 1984). The microparticle concentration decreases for diameters larger than 0.52 μm and increases slightly for diameters between 3.17 and 5.04 μm . So the

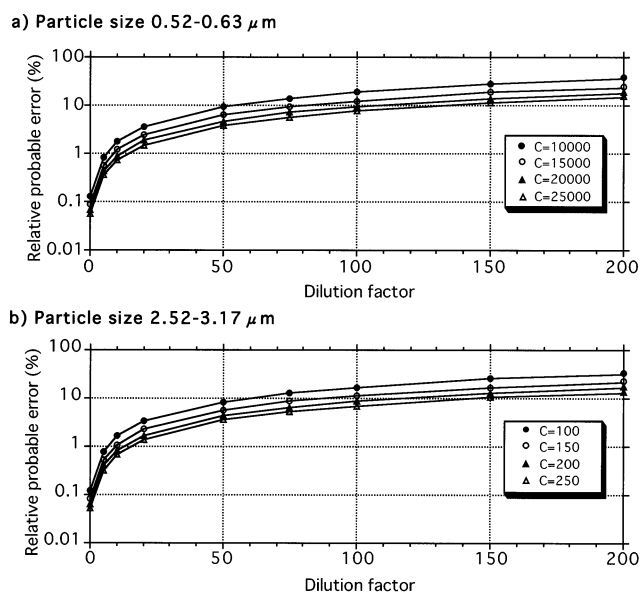


Fig. 6. Probable error of microparticle number measurement with a laser particle counter estimated by the law of propagation of errors. The probable errors for small microparticles with size of a) 0.52–0.63 μm and b) 2.52–3.17 μm are less than 10% when the molten sample is diluted 50 times or less by ultrapure water.

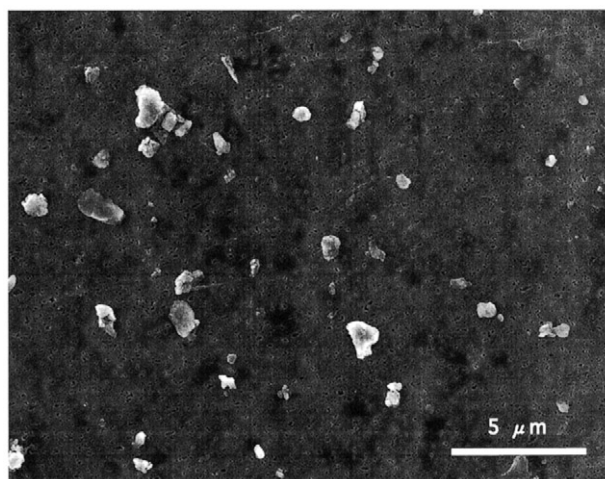


Fig. 7. SEM image of microparticles at 521 m depth of the Dome Fuji ice core to evaluate the measurement coincidence loss of the sample diluted by 50 times.

volume concentration increases considerably with diameter larger than 3.17 μm . Figures 8b and 8c show the comparison of size-number and size-volume distributions of particles larger than 0.52 μm in diameter, which is within the measurement range of the laser particle counter, obtained by SEM image analysis and the laser counter method. The relative number and relative volume concentrations are shown in these figures. If we consider the fact that the

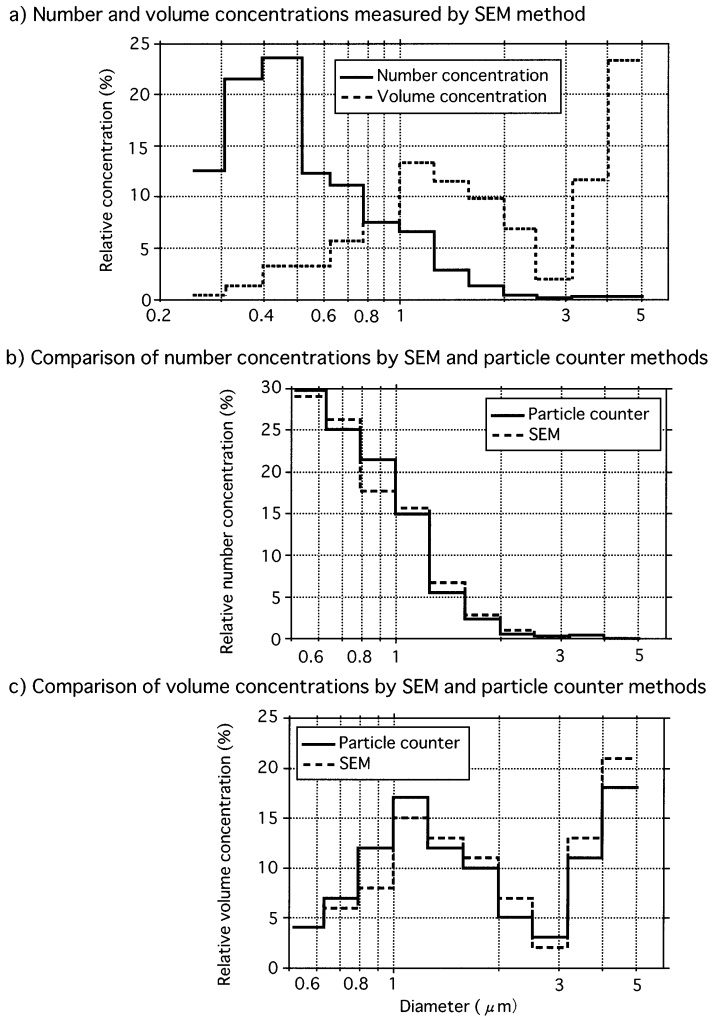


Fig. 8. a) Size-number and size-volume distributions of microparticles larger than $0.25 \mu\text{m}$ in diameter based on the SEM image magnified 7000 times. The number concentration has a peak in the size range between 0.40 and $0.52 \mu\text{m}$. The volume concentration has a peak in the size range between 1 and $2 \mu\text{m}$ and increases considerably with diameter larger than $3.17 \mu\text{m}$. b) Comparison of size-number distribution of particles larger than $0.52 \mu\text{m}$ in diameter obtained by SEM image analysis and the laser counter method. c) Comparison of size-volume distribution of particles as in b).

SEM images used are within the limited range of 0.002% of the total filtered area, the particle size distribution based on SEM images agrees well with the particle size distribution measured by the laser particle counter.

2.2.7. Analytical method

Prior to the measurement, the concentration of the microparticles contained in ultrapure water in a washed glass bottle is measured. If the particle concentration is within 100 particles per ml , sample measurement is performed. If the concentration is higher than this value, the glass bottle is washed again or ultrapure water is well circulated through a reverse osmo-

sis system (Milli-Q SP TOC, Millipore Co.) to purify the water. Then, ultrapure water is collected again, and microparticles in the ultrapure water are measured. Into this glass bottle, 50 ml of ultrapure water with microparticle concentration of 100 particles/ml or less is injected using a pipette, and the weight is determined with the accuracy of 0.01 g. Then, into this glass bottle, about 1 ml of the molten sample is injected using an auto-pipette, and the weight is determined in the unit of 0.01 g. Taking special care not to intermingle air bubbles, the bottle is shaken to mix the ultrapure water with the sample. Then, measurement is made using the laser particle counter. The flow rate of the sample sent to the sensor is 50 ml min^{-1} , and measurements can be performed for two seconds at one-second intervals more than 20 times for one sample. Because measurement error may be involved due to intermingling of air bubbles in the first few measurements and in the last measurement, the minimum measurement result is adopted from all measurement data excluding these. From the results of this measurement, the microparticles contained in the ultrapure water used for dilution are subtracted as blank, and this is regarded as the microparticle concentration data of the sample. The measurement was made by setting the measurement range to 10 channels, namely, $0.52\text{--}0.63 \mu\text{m}$, $0.63\text{--}0.79 \mu\text{m}$, $0.79\text{--}1.00 \mu\text{m}$, $1.00\text{--}1.26 \mu\text{m}$, $1.26\text{--}1.59 \mu\text{m}$, $1.59\text{--}2.00 \mu\text{m}$, $2.00\text{--}2.52 \mu\text{m}$, $2.52\text{--}3.17 \mu\text{m}$, $3.17\text{--}4.00 \mu\text{m}$, and $4.00\text{--}5.04 \mu\text{m}$.

3. Results and discussion

Concentration and size distribution of microparticles in the Dome Fuji ice core were measured on 2829 samples. The sample length is 6–8 cm cut at 0.5–1.0 m depth intervals to have 100–200 year time resolution.

3.1. Concentration of microparticles

Figure 9 shows the profile of oxygen isotopic ratio of the Dome Fuji ice core for the past 320 k-years, and profiles of number and volume concentrations of the microparticles. The number concentration represents the total number of microparticles in 1 ml of meltwater sample in the particle size range of $0.52 \mu\text{m}$ to $5.04 \mu\text{m}$ when it is assumed that each particle is spherical. The oxygen isotopic ratio profile and age of the core were quoted from Watanabe *et al.* (1999) and Watanabe *et al.* (2003), respectively. Cold and warm climate stages are indicated in the figure based on the oxygen isotopic ratio profile. The oxygen isotopic ratio in each glacial cycle is not always the same but follows a similar pattern; the same alphabetical letter indicates corresponding climate stages.

The concentration profile of microparticles shows several features:

- 1) The most obvious feature is that the concentration is highest in the coldest stages (B, B', and D'') of the glacial and is low in the Holocene (A) and the interglacials (A', A'', and A''').

- 2) The concentration is still low even in the early cold climate stage (F, F', and F'') of the glacials. Also, the climatic condition shown by the oxygen isotope ratio was almost equal in climate stages B and D as well as B' and D', but the concentration of microparticles reached the highest value in the last cold period (B and B') in the glacial when the sea level was lowered most. This may be explained by the fact that microparticle transport onto the Antarctic ice sheet does not only depend on the climatic condition but also on the extent of microparticle source areas surrounding Antarctica, the major source area being Patagonia

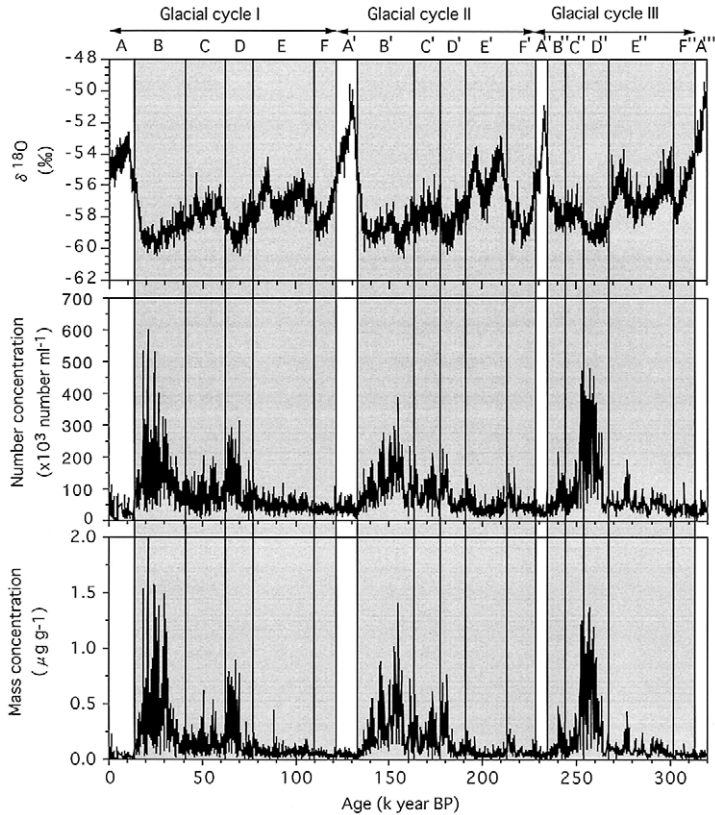


Fig. 9. Profile of oxygen isotopic ratio of Dome Fuji ice core for the past 320 k-years (Watanabe *et al.*, 1999), and profiles of number and mass concentrations of the microparticles. The mass concentration is expressed in $\mu\text{g g}^{-1}$ assuming a dust density of 2500 kg m^{-3} . Climate stages are shown in the figure based on the oxygen isotopic ratio profile.

(De Angelis *et al.*, 1992; Grousset *et al.*, 1992; Basile *et al.*, 1997; Iriondo, 2000).

3) In glacial cycle III, a major peak of microparticle concentration appeared only once in climate stage D'', which is different from the other glacial cycles. In the climatic condition shown by the oxygen isotopic ratio, stage B'' in the last stadial of the antepenultimate glacial is not the coldest. Microparticle concentration reached the peak value in stage D'', this suggests that the sea level may have decreased the most during this period and the continental shelf was extensively exposed to the air in the southern part of South America.

4) Comparing peak values of the microparticle mass concentration of the glacials in the Dome Fuji core with those of the Vostok core, Dome Fuji peaks of $1.1\text{--}1.5 \mu\text{g g}^{-1}$ coincide well with the Vostok values of $1.0\text{--}1.6 \mu\text{g g}^{-1}$ (Petit *et al.*, 1999). This suggests that dust transport from the source area to these Antarctic inland places and snow accumulation during the coldest period of the glacials were not so different from each other.

5) It is evident from Fig. 10 that the concentration of microparticles in the Dome Fuji ice core does not depend linearly on air temperature. In Fig. 10, the values were obtained from the oxygen isotopic ratio and microparticle number concentration profile shown in Fig. 9

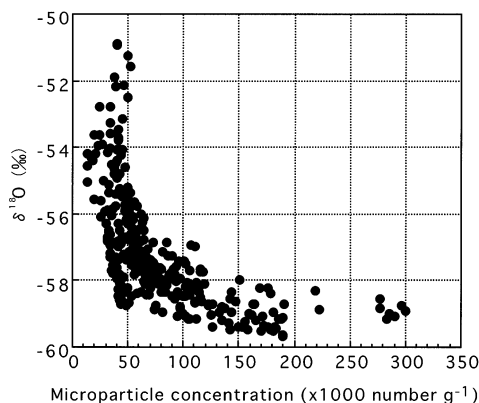


Fig. 10. Relation between $\delta^{18}\text{O}$ and microparticle number concentration at every 1000 years extracted from both smoothed profiles by cutting off the 5000 year or less fluctuations. This figure suggests that air temperature change is not associated with the changes in microparticle number concentration, which depends both on air transport ability and dust source environment.

by cutting off the 5000 year or less fluctuations and by averaging data for every 1000 years. From this figure, it is clear that the microparticle concentration is in the range of approximately 10000–50000 particles per ml in the warm period when the oxygen isotopic ratio was -56‰ or more. The warm periods of -56‰ or more include the Holocene (A) and interglacial periods (A', A'' and A''') as well as the initial interstadials of each glacial (E, E' and E''). During these periods, the decrease of sea level was not yet extreme, and the source area from which microparticles were generated was not very different from that of the interglacial. Furthermore, these results suggest that the air temperature change in the warm period was not associated with great changes in the ability to transport aeolian dust.

In cold periods when the oxygen isotopic ratio was less than -58‰ , microparticle concentration fluctuated independently of air temperature. The cold period with oxygen isotope ratio less than -58‰ corresponded to the middle and final stadials in the glacial. Microparticle concentrations during these periods show extensive change; this may be attributed to enhanced exposure of the continental shelf due to the sea level lowering.

3.2. Size distribution of microparticles

The profiles of number concentration for 10 particle size ranges are presented in Fig. 11. In this figure, climate stages are the same as shown in Fig. 9. The concentration of microparticles smaller than $1.26\ \mu\text{m}$ shows a peak value exceeding 50000 particles per ml in the final stadial of the glacial and also shows several thousands/ml or more even in the climate stages when the concentration is decreased such as during an interglacial or early stadial of a glacial. On the other hand, microparticles larger than $1.26\ \mu\text{m}$ show high concentrations in the climate stages in the latter half of the glacial (B, C, D and the corresponding stages), but decrease to several thousands per ml in the other climate stages. For larger microparticles with diameters of more than $2\ \mu\text{m}$, the concentration is lower than several hundreds per ml in the last stadial of the glacial. In the other climate stages, concentration decreased to several hundred/ml or lower.

In order to facilitate explanation of the features of the size distribution, all measured samples were averaged to one size distribution. The average number distribution is shown in Fig. 12 together with the standard deviation and the relative standard deviation. The number concentration decreases with increase of size as shown in this figure. The maximum concentration appears in the particle range 0.40 to $0.52\ \mu\text{m}$ based on SEM image analysis (Fig. 5).

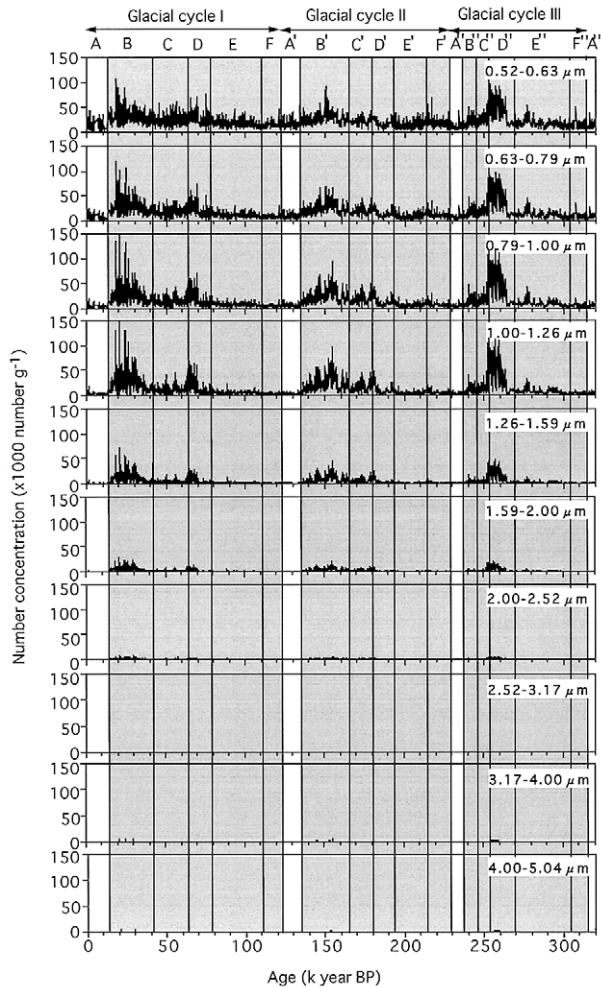


Fig. 11. Profiles of microparticle number concentration for 10 particle size ranges through 3 glacial cycles. This figure shows that the fluctuation of smaller microparticles is small through the glacial cycles.

Also, for microparticles larger than $2.00\ \mu\text{m}$, number concentration reaches the minimum value at $2.52\text{--}3.17\ \mu\text{m}$, and a small peak appears at $3.17\text{--}4.00\ \mu\text{m}$. The characteristics of the size distribution of microparticles larger than $2.00\ \mu\text{m}$ will be discussed later.

The standard deviation of the average microparticle concentration throughout the glacial cycles is approximately $15000\text{--}17500$ particles per ml for particles between 0.52 and $1.26\ \mu\text{m}$, while it decreases considerably for particles larger than $1.26\ \mu\text{m}$. However, the relative deviation increases with particle size and is almost constant for particles larger than $2\ \mu\text{m}$.

An overview of the characteristics of particle size distribution for each climate stage is shown in Fig. 13. This figure represents average volume concentration at each of the climate stages. The feature of volume concentration common to all climate stages in each glacial cycle is modal diameter of $1.00\text{--}1.26\ \mu\text{m}$ for particles with diameter smaller than $3\ \mu\text{m}$. This

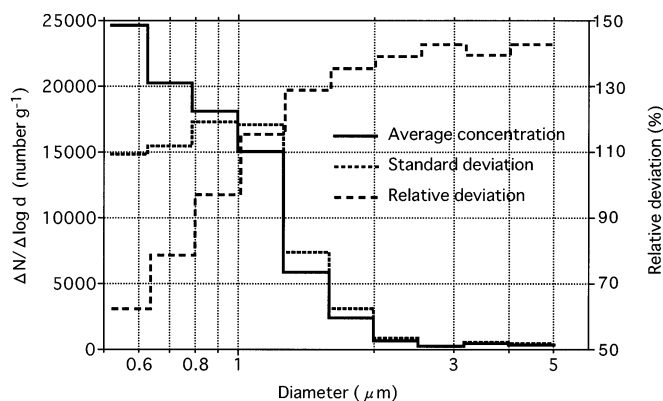


Fig. 12. Average size distributions for number concentration, standard deviation and relative standard deviation (standard deviation/average number concentration;%) in each climate stage of the glacial cycles.

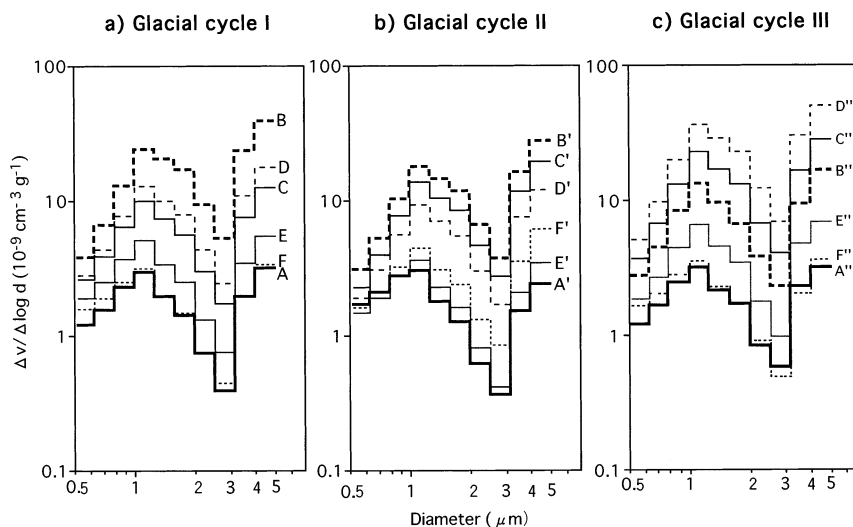


Fig. 13. Characteristics of particle volume-size distribution for each climate stage. The feature common to all climate stages in each glacial cycle is that there is a peak in the particle size range of 1.00–1.26 μm and a minimum in the particle size range of 2.52–3.17 μm , and it increases with particle size larger than this. The dynamic range in each particle size tends to increase with size due to greater increase of larger particles during cold climate stages of the later glacial, probably by enhanced wind speed over the dust source area and enhanced atmospheric circulation.

mode is different from the microparticles in the Dome C ice core (Petit *et al.*, 1981; Delmonte *et al.*, 2002) which has a peak at around 2 μm diameter.

The volume concentration of the microparticles has a minimum value for particles of 2.52–3.17 μm and it increases with particle size larger than this. The tendency of volume concentration reaching the minimum in relatively larger particle size and increasing thereafter with size is also found in the size distribution of microparticles in the 22 m deep core from Northern Victoria Land, Antarctica (Maggi and Petit, 1998) and the GRIP deep ice

core, Greenland (Steffensen, 1997). In the core of Victoria Land, volume concentration of particles reaches the minimum in particle size of 3–4 μm in radius and it increases with particle size larger than this. Maggi and Petit (1998) point out that particles larger than 3–4 μm in radius may have originated from a local source and may have been transported over a short distance. The increase of volume concentration seen in the particles larger than 3.17 μm in the Dome Fuji ice core may have been caused by particles originating from the Antarctic continent in the interglacial, the interstadials and the initial stadial of the glacial. On the other hand, the increase in the middle and the late stadials of the glacial may have been caused by enhanced transport of aeolian dust onto the Antarctic ice sheet from a Patagonian continental shelf that was extensively exposed due to sea level lowering.

The dynamic range of volume concentration in each particle size tends to increase with diameter as shown in Fig. 13. This means that transportation of smaller particles was relatively constant through the glacial cycle but transportation of larger ones increased relatively during colder stages of the late glacial, probably due to enhanced wind speed over the dust source area and enhanced atmospheric circulation.

4. Conclusion

In the present study, we verified the usefulness and the features of an analytical method to measure the concentration and size distribution of microparticles in an ice core using a light-scattering laser particle counter, and we obtained the following results on concentration and size distribution of microparticles in the deep ice core from Dome Fuji, Antarctica.

1) By using the laser-light scattering method, it is possible to measure the concentration and size distribution of microparticles without pre-treatment and in an easy manner by diluting the sample with ultrapure water by 50 times. Analytical accuracy by this 50-times dilution method is estimated to be 10% based on the law of propagation of errors. Also, we can select the laser particle counter method since it requires less attention for pre-treatment of the samples compared with the method using a Coulter Counter.

2) In glacial cycles I and II, air temperature was almost equal in the last two stadials, while the concentration of microparticles reached a peak in the last stadial of the glacial. This may be because the concentration of microparticles greatly depended on environmental conditions of the particle source area around Antarctic continent such as the area of continental shelves exposed to the air, in addition to air temperature, which may have exerted influence on the air transport ability of aeolian dust.

3) In warm periods with oxygen isotopic ratio more than -56% (interglacials including the Holocene and interstadials of the glacial), the concentration of microparticles did not follow the changes of air temperature and remained at almost the same low level. This suggests that air temperature did not cause the changes in air ability to transport aeolian dust or in the dust source area during this period. In cold periods when the oxygen isotopic ratio was -58% or lower (stadials in the glacial), the concentration of microparticles shows a change without regard to the change of air temperature. This may suggest that the quantity of microparticles transported to the Antarctica during this period primarily depended upon the change in area of continental shelves extensively exposed by sea level lowering.

4) The size distribution of microparticles in volume concentration as seen throughout the glacial cycles is characterized by a peak in the particle size range of 1.00–1.26 μm and by

an increase with particle size of 3.17–4.00 μm or more. The increase of volume concentration in the particle size of 3.17–4.00 μm or more may indicate the possibility that it was caused by microparticles which originated Antarctic continent in interglacials, interstadials and initial stadial of the glacial. The increase of volume concentration in the middle and the late stadials in the glacial may have been caused by enhanced aeolian dust generation by strong winds blown from the continental shelves exposed by sea level lowering in these periods.

5) Dynamic range of volume concentration in each particle size tends to increase with diameter. This may be caused by much enhanced transportation of larger particles during colder stages of the late glacial probably due to the enhanced wind speed over dust source area and enhanced atmospheric circulation.

Acknowledgments

For carrying out the present study, we owed many persons for their assistance and cooperation. In particular, we owed much to the devoted assistance offered from JARE members for the deep ice coring at Dome Fuji and Ms. Tomoko Naka of National Institute of Polar Research for the analysis of microparticles using a laser-light scattering particle counter, to Prof. Kokichi Kamiyama, Dr. Makoto Igarashi and Dr. Yoshinori Iizuka (present affiliation: Yuge National College of Maritime Technology) of the National Institute of Polar Research for their cooperation in sample preparation and laboratory management, and many other persons. We extend sincere gratitude to these persons for their kind support for the present study. We are also grateful to Dr. Urs Ruth of the University of Heidelberg for his valuable comments on the manuscript. This study was supported by a Grant-in-Aid for Scientific Research (No. 10204101; Principal Investigator: Dr. Okitsugu Watanabe) from the Ministry of Education, Culture, Sports, Science and Technology, Japan.

References

- Basile, I., Grousset, F.E., Revel, M., Petit, J.R., Biscaye, P.E. and Barkov, N.I. (1997): Patagonian origin of glacial dust deposited in East Antarctica (Vostok and Dome C) during glacial stages 2, 4 and 6. *Earth Planet. Sci. Lett.*, **146**, 573–589.
- Biscaye, P.E., Grousset, F.E., Revel, M., Van der Gaast, S., Zielinski, G.A., Vaars, A. and Kukla, G. (1997): Asian provenance of glacial dust (stage 2) in the Greenland Ice Sheet Project 2 ice core, Summit, Greenland. *J. Geophys. Res.*, **102** (C12), 26765–26781.
- De Angelis, M., Legrand, M.R., Petit, J.R., Barkov, N.I. and Korotkevitch, Te. S. (1984): Soluble and insoluble impurities along the 950 m deep Vostok ice core (Antarctica)-Climatic implications. *J. Atmos. Chem.*, **1**, 251–239.
- De Angelis, M., Barkov, N.I. and Petrov, V.N. (1992): Sources of continental dust over Antarctica during the last glacial cycle. *J. Atmos. Chem.*, **14**, 233–244.
- Delmonte, B., Petit, J.R. and Maggi, V. (2002): Glacial to Holocene implications of the new 27000-year dust record from the EPICA Dome C (East Antarctica) ice core. *Clim. Dyn.*, **18**, 647–660.
- Fujii, Y. and Ohata, T. (1982): Possible causes of the variation in microparticle concentration in an ice core from Mizuho Station, Antarctica. *Ann. Glaciol.*, **3**, 107–112.
- Fujii, Y. and Watanabe, O. (1988): Microparticle concentration and electrical conductivity of a 700 m core from Mizuho Station, Antarctica. *Ann. Glaciol.*, **10**, 38–42.
- Fujii, Y., Kamiyama, K., Shoji, S., Narita, H., Nishio, F., Kameda, T. and Watanabe, O. (2001): 210-year ice core records of dust storm, volcanic eruption and acidification at Site-J, Greenland. *Mem. Natl Inst. Polar Res.*,

- Spec. Issue, **54**, 209–220.
- Gliozzi, J. (1966): Size-distribution analysis of microparticles in two Antarctic firn cores. *J. Geophys. Res.*, **71**, 1993–1998.
- Grousset, F.E., Biscaye, P.E., Revel, M., Petit, J.R., Pye, K., Joussaume, S. and Jouzel, J. (1992): Antarctic (Dome C) ice-core dust at 18 k.y. B.P.: Isotopic constraints on origin. *Earth Planet. Sci. Lett.*, **111**, 175–182.
- Hammer, C.U. (1977): Dust studies on Greenland ice cores. *IAHS Publ.*, **118**, 365–370.
- Iriondo, M. (2000): Patagonian dust in Antarctica. *Quat. Int.*, **68–71**, 83–83.
- Maggi, V. and Petit, J.R. (1998): Atmospheric dust concentration record from the Hercules Neve firn core, northern Victoria Land, Antarctica. *Ann. Glaciol.*, **27**, 355–359.
- Met One (1991): Light-scattering laser sensors for liquid. Met One Product Note, January 17.
- Mosley-Thompson, E. and Thompson, L.G. (1982): Nine centuries of microparticle deposition at the South Pole. *Quat. Res.*, **17**, 1–13.
- Mumford, J.W. and Peer, D.A. (1982): Microparticles, marine salts and stable isotopes in a shallow firn core from the Antarctic Peninsula. *Br. Antarct. Surv. Bull.*, **56**, 37–47.
- Petit, J.R., Briat, M. and Royer, A. (1981): Ice age aerosol content from East Antarctic ice core samples and past wind strength. *Nature*, **293**, 857–859.
- Petit, J.R. and 18 others (1999): Climate and atmospheric history of the past 420,000 years from the Vostok ice core, Antarctica. *Nature*, **399**, 429–436.
- Ram, M. and Koening, G. (1997): Continuous dust concentration profile of pre-Holocene ice from the Greenland Ice Sheet Project 2 ice core: Dust stadials, interstadials, and the Eemian. *J. Geophys. Res.*, **102** (C12), 26641–26648.
- Royer, A., De Angelis, M. and Petit, J.R. (1983): A 30000 year record of physical and optical properties of microparticles from an east Antarctic ice core and implications for paleoclimate reconstruction models. *Clim. Change*, **5**, 381–412.
- Ruth, U. (2002): Concentration and size distribution of microparticles in the NGRIP ice core (Central Greenland) during the last glacial period. *Ber. Polar-Meerforschung.*, **428**, 146 p.
- Ruth, U., Wagenbach, D., Bigler, M., Steffensen J.P. and Rothlisberger, R. (2002): High resolution microparticle profiles at NGRIP: case studies of the calcium-dust relationship. *Ann. Glaciol.*, **35**, 237–242.
- Steffensen, J.P. (1988): Analysis of the seasonal variation in dust, Cl^- , NO_3^- , and SO_4^{2-} in two central Greenland firn cores. *Ann. Glaciol.*, **10**, 171–177.
- Steffensen, J.P. (1997): The size distribution of microparticles from selected segments of the Greenland Ice Core Project ice core representing different climatic periods. *J. Geophys. Res.*, **102** (C12), 26755–26763.
- Thompson, L.G. and Mosley-Thompson, E. (1981): Temporal variability of microparticle properties in polar ice sheet. *J. Volcanol. Geotherm. Res.*, **11**, 11–27.
- Thompson, L.G., Hamilton, W.L. and Bull, C. (1975): Climatological implications of microparticle concentrations in the ice core from “BYRD” station, Western Antarctica. *J. Glaciol.*, **14**, 433–444.
- Zielinski, G.A. and Mershon, G.R. (1997): Paleoenvironmental implications of the insoluble microparticle record in the GISP2 (Greenland) ice core during the rapidly changing climate of the Pleistocene-Holocene transition. *Geol. Soc. Am. Bull.*, **109**, 547–559.
- Watanabe, O., Fujii, Y., Kamiyama, K., Motoyama, H., Furukawa, T., Igarashi, M., Kohno, M., Kanamori, S., Kanamori, N., Ageta, Y., Nakawo, M., Tanaka, H., Satow, K., Shoji, H., Kawamura, K., Matoba, S. and Shimada, W. (1999): Basic analyses of Dome Fuji deep ice core Part 1: Stable oxygen and hydrogen isotope ratios, major chemical compositions and dust concentration. *Polar Meteorol. Glaciol.*, **13**, 83–89.
- Watanabe, O., Shoji, H., Satow, K., Motoyama, H., Fujii, Y., Narita, H. and Aoki, S. (2003): Dating of the Dome Fuji, Antarctica deep ice core. *Mem. Natl Inst. Polar Res., Spec. Issue*, **57**, 25–37.

(Received December 26, 2002; Revised manuscript accepted February 3, 2003)